Singular Vectors: The Effect of Spatial Scale on Linear Growth of Disturbances

D. L. HARTMANN,* R. BUIZZA, AND T. N. PALMER

European Centre for Medium-Range Weather Forecasts, Reading, England

(Manuscript received 23 January 1995, in final form 9 May 1995)

ABSTRACT

The scale dependence of rapidly growing perturbations is investigated by studying the dominant singular vectors of T21 and T42 versions of the ECMWF model, which show the most linear energy growth in a 3-day period. A spectral filter is applied to the optimization process to determine which spatial scales are most effective in promoting energy growth. When the initial perturbation is confined to the top half of the total spherical harmonic wavenumber spectrum (high wavenumber end), the growth rates and final structures of the disturbances are changed very little from the case in which all wavenumbers are included. These results indicate that synoptic waves that become fully developed in a period of three days can arise from initial perturbations that are entirely contained at subsynoptic scales. Rapid growth is associated with initial perturbations that consist of smaller spatial scales concentrated near the effective steering level. The linear evolution of these initial perturbations in a highly complex basic flow leads to disturbances of synoptic scale that extend through most of the depth of the troposphere. Growth rates are approximately doubled when the model resolution is increased from T21 to T42, which is consistent with greater growth being associated with smaller spatial scales. When the initial perturbation is confined to the lower half of the total wavenumber spectrum, which describes the larger horizontal scales, the growth rates are significantly reduced and the initial and final structures are very different from the case in which all wavenumbers are included. These low wavenumber perturbations tend to be more barotropic in structure and in growth characteristics. As expected from their linear growth rates, when the low-wavenumber perturbations are inserted in the T63 forecast model, they grow more slowly and result in less forecast dispersion than the high wavenumber perturbations.

1. Introduction

A number of recent studies have investigated linear perturbations to atmospheric flow that are determined from the constraint that they produce the maximum possible increase in some amplitude norm over a finite interval of time. These finite-time optimal perturbations have been investigated in analytical studies (Farrell 1982, 1989; Boyd 1983) and in numerical models with a limited number of degrees of freedom (Lacarra and Talagrand 1988; Borges and Hartmann 1992; Molteni and Palmer 1993). Recently Buizza et al. (1993) have described the calculation of what can be called the singular vectors of a T21L19 version of the ECMWF forecast model. Buizza (1994) has described the sensitivity of these growing structures to the details of their calculation. Buizza and Palmer (1995) have related singular vectors to normal modes, their adjoints, and other measures of linear growth, and have also described the singular vector structure in relation to wintertime circulation.

Singular vectors are calculated by optimizing the growth of linear perturbations about the evolving state of the forecast model over some finite time. In contrast to normal modes, singular vectors form an orthogonal set of structures, and these can be ordered according to growth rate, with the fastest growing structure being the first singular vector, and so on to the last. These structures are defined for both the initial time and the final time, so that the evolution of the growing structures can be easily shown. The structures tend to be localized in regions that normal-mode instability theory would identify as being relatively unstable to baroclinic waves, and they often have the structure of synoptic-scale wave packets. Their growth rates over the finite time interval of the optimization problem are greater than that of normal modes, and their structures are more local. The structures are relatively insensitive to modest changes in optimization time. For example, one gets similar basic structures for optimization times between 1.5 and 3 days. Also, the singular vector structures are not very sensitive to the geographic domain for which the optimization is performed, provided that domain includes the natural location of the structure, which appears to be a characteristic of the flow configuration. For example, if one finds a singular vector that grows

* Permanent affiliation: Department of Atmospheric Sciences, University of Washington, Seattle, Washington.

Corresponding author address: Dr. Dennis L. Hartmann, Department of Atmospheric Sciences, University of Washington, Box 351640, Seattle, WA 98195.

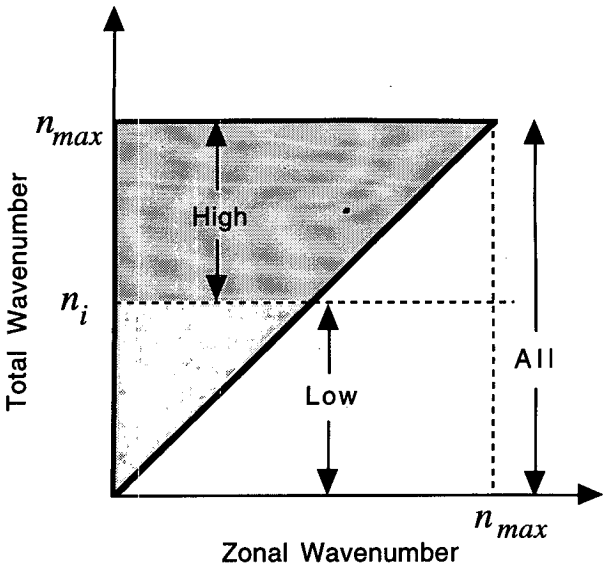

FIG. 1. Diagram showing the triangular truncation of the spherical harmonic expansion with maximum total wavenumber n_{max} and intermediate total wavenumber n_i.

on the Pacific jet, the structure of that singular vector will be the same whether the optimization area is the Northern Hemisphere or just that part of the Pacific where the singular vector exists.

It is hypothesized that the singular vectors compose a useful and meaningful set of basic dynamical structures. Because they form an orthogonal and complete[1] set of structure functions ordered according to growth potential, it is expected that the linear evolution of an arbitrary initial perturbation will be dominated by its projection onto the dominant singular vectors. Given an ensemble of random initial perturbations, we expect that the perturbations at the end of the optimization time will be efficiently described by the subset of the fastest-growing, or dominant, singular vectors. The dominant singular vectors thus contain much of the information about linear growth, and their location and spatial structure are of fundamental interest.

Buizza and Palmer (1995) described how the dominant singular vectors constructed with an energy norm evolve from small scales to large scales between initial and final time, and suggested that this might be related to the "butterfly effect" (Lorenz 1963) and ultimately to issues of predictability. In this paper we present some calculations to clarify the role of small-scale disturbances leading to efficient growth of energy at synoptic scales. This is done by applying a spherical harmonic total wavenumber filter to the optimization problem, which enables us to illustrate more clearly the critical role of small scales in the initial perturbation and the efficient manner in which this energy can cascade to synoptic scales during the linear evolution of perturbations on a realistic flow. We also look at the case in which the initial perturbation is confined to large scales. In this case the growth rates are much slower and the growth occurs not in the low wavenumbers alone, but also in higher wavenumbers, so that the evolved singular vectors at final time have their dominant structures at smaller scales than the initial perturbations. Some nonlinear calculations with a T63 version are performed to show that the large-scale features are not preserved, but evolve into smaller-scale wavetrains downstream. These wavetrains are of smaller amplitude than they would be if they had been initiated from singular vectors with the same initial energy, but constructed by allowing the smaller scales to contribute.

2. Calculation of singular vectors with spatial and spectral windowing

In this paper we will examine the scale dependence of singular vector structure by using a spectral filter to constrain the optimization problem. In this way we may separately constrain the initial perturbation to be composed of a limited portion of the total wavenumber spectrum and ask that the final state growth be optimized for an independent portion of the total wavenumber spectrum. In all of the cases described in this paper, total energy will be used as the optimization norm. The spectral filter is illustrated schematically in Fig. 1, which shows the wavenumber diagram for a spherical harmonic representation with triangular truncation. The total wavenumber spectrum can be cut at the intermediate wavenumber n_i, so that the total field is divided into a low wavenumber and a high wavenumber region. Since the spectral filter can be applied to both the initial perturbation and to its final evolved state at the optimization time, a total of nine spectral filtering experiments is possible, as indicated in Table 1. By investigating the growth rates and structures as-

TABLE 1. Nine possible cases with a single intermediate total wavenumber cut at $n = n_i$ within a total wavenumber range of $n = 0$ to $n = n_{max}$.

Case	Initial wavenumber range	Final wavenumber range	Description
1	$0-n_{max}$	$0-n_{max}$	all to all
2	$0-n_{max}$	$n_{i+1}-n_{max}$	all to high
3	$0-n_{max}$	$0-n_i$	all to low
4	$n_{i+1}-n_{max}$	$0-n_{max}$	high to all
5	$n_{i+1}-n_{max}$	$n_{i+1}-n_{max}$	high to high
6	$n_{i+1}-n_{max}$	$0-n_i$	high to low
7	$0-n_i$	$0-n_{max}$	low to all
8	$0-n_i$	$n_{i+1}-n_{max}$	low to high
9	$0-n_i$	$0-n_i$	low to low

[1] Complete in the sense that any arbitrary disturbance that can be resolved by the model can be expressed as a linear combination of singular vectors.

sociated with these nine possible cases, we can investigate which wavenumbers contain the greatest potential for growth and also how the structure changes when the total wavenumber is constrained.

Hereafter, we briefly review the methodology applied to compute the singular vectors. We refer to Buizza et al. (1993) and to Buizza and Palmer (1995) for a more complete treatment. The full nonlinear model, the linear version, and its adjoint used to compute the singular vectors are components of the ECMWF Integrated Forecasting System, developed in collaboration with Météo-France (Courtier et al. 1991).

a. Singular vector computation

Denote by $A[x]$ the ECMWF nonlinear primitive equation model. The time evolution equation for a state vector x can be formally written in terms of the (M dimensional) nonlinear evolution equation

$$\frac{\partial x}{\partial t} = A[x], \tag{1}$$

where the components of the state vector x are the spherical-harmonics expansions of vorticity ζ, divergence D, temperature T, humidity q, together with the logarithm of surface pressure π.

Consider a small perturbation x' of the state vector x. For sufficiently short time intervals, its evolution can be described by the linear model

$$\frac{\partial x'}{\partial t} = A_l x', \tag{2}$$

where A_l is an approximation of the tangent linear model $\partial A/\partial x|_{x(t)}$. In fact, while a complete linearization of the model dynamics can be included, the only physical processes included in the linear operator A_l are simplified versions of the ECMWF vertical diffusion and surface drag schemes and horizontal diffusion (Buizza 1994). The present study thus includes primarily dynamical processes. The linearization and inclusion of more of the physics of the model would probably change the results somewhat, particularly at the smallest scales. The horizontal diffusion is a ∇^4 scheme with the coefficient chosen so that the e-folding time of the highest wavenumber is 5 days for T21 and 1.25 days for T42. The diffusion is slow compared to the dynamical processes in the T21 case, and in the T42 case a doubling of the diffusion coefficient reduces the growth rate by only about 20%, although it does have the effect of removing some apparently unphysical high wavenumber initial perturbations. We therefore argue that our general conclusions are not overly sensitive to the diffusion coefficient, although the initial energy shifts toward smaller scales as the diffusion is reduced.

Equation (2) can be written in the integral form

$$x'(t) = L(t, t_0)x'(t_0). \tag{3}$$

The operator $L(t, t_0)$ is referred to as the forward tangent propagator; it maps small perturbations along the (nonlinear) trajectory from an initial time t_0 to some future time t. From here on we drop the "primes" on the perturbation quantities. The propagator L is itself compounded from the individual operators L_{NNMI}, L_{dyn}, L_{phys}. These denote, respectively, the action of the nonlinear normal mode initialization (NNMI) procedure (see Buizza et al. 1993) and, for each time step, the action of the adiabatic part of the model equations and of the physical parameterization processes. More precisely, $L(t_N, t_0)$ on an initial state $x(t_0)$ in (3) can be decomposed as

$$[\prod_{n=1}^{n=N} L_{\text{phys}}(t_n, t_{n-1})L_{\text{dyn}}(t_n, t_{n-1})]L_{\text{NNMI}}(t_0)x(t_0), \tag{4}$$

where $t_n - t_{n-1} = \delta t$, the model time step.

We can define an inner product $(\cdot\,;\,\cdot)$ based on the total perturbation energy; that is,

$$(x; y) = \frac{1}{2}\int_0^1 \int_s \Big(\nabla\Delta^{-1}\zeta_x \cdot \nabla\Delta^{-1}\zeta_y + \nabla\Delta^{-1}D_x \cdot \nabla\Delta^{-1}D_y + RT_r \ln\pi_x \ln\pi_y + \frac{C_p}{T_r} T_x T_y \Big) d\Sigma \Big(\frac{\partial p}{\partial \eta}\Big) d\eta, \tag{5}$$

where η is the terrain-following vertical coordinate used in the ECMWF model.

Using (3) the perturbation norm at time t is given by

$$\|x(t)\|^2 \equiv [x(t); x(t)] = [x(t_0); L^{*E}Lx(t_0)], \tag{6}$$

where L^{*E} is the adjoint of L with respect to the energy inner product. Unlike L itself, the operator $L^{*E}L$ is symmetric. Hence, its eigenvectors $\mathbf{v}_i(t_0)$ can be chosen to form a complete orthonormal basis in the M-dimensional tangent space of linear perturbations with real eigenvalues $\sigma_i^2 \geq 0$ (e.g., Noble and Daniel 1977); that is,

$$(L^{*E}L)\mathbf{v}_i(t_0) = \sigma_i^2 \mathbf{v}_i(t_0). \tag{7}$$

Since any $x(t)/\|x(t_0)\|$ can be written as a linear combination of the set $\mathbf{v}_i(t)$, it follows that

$$\max_{x(t_0)\neq 0}[\|x(t)\|/\|x(t_0)\|] = \sigma_1. \tag{8}$$

The σ_i, ranked in terms of magnitude, are called the singular values of the operator L, and the vectors $\mathbf{v}_i(t)$ are called the singular vectors of L. Maximum energy growth over the time interval $t - t_0$ is therefore associated with the dominant singular vector: $\mathbf{v}_1(t_0)$ at initial time and $\mathbf{v}_1(t)$ at optimization time. In all of the computations described here the optimization time was taken to be three days.

b. The local projection operator

The energy inner product (5) is defined through integration of perturbation quantities over the whole at-

mosphere, and so the singular vectors are defined to maximize global energy. A local projection operator (Buizza and Palmer 1995) can be defined to constrain, to a restricted geographical region, the area in which the energy of the singular vector at final time is maximized.

As mentioned above, the components of the state $x(t)$ are largely defined in spectral space. Let S represent the spectral to gridpoint transform and define a "hat" function

$$g(p) = 1 \quad \text{if} \quad p \in \Sigma, \tag{9a}$$

$$g(p) = 0 \quad \text{if} \quad p \notin \Sigma, \tag{9b}$$

where p is a point and Σ is a specified local region in physical space. Denote by Gx_G the multiplication of a vector x_G, defined in physical space, by the hat function.

The local projection operator T is defined as

$$T \equiv S^{-1}GS. \tag{10}$$

Perturbations chosen for growth inside Σ can be computed by applying T after the linear integration

$$\|x(t)\|^2 = [Tx(t); Tx(t)] = [x(t_0); L^{*E}T^{*E}TLx(t_0)], \tag{11}$$

where T^{*E} is the adjoint of the local projection operator with respect to the energy inner product. The singular values of the operator TL give the amplification, within the target region, of perturbations with initial unit amplitude in the global energy norm. As with global singular vectors, perturbations produced using the local projection operator are orthogonal in the global sense. In all of the computations described here, the geographical domain in which the final energy was maximized was taken to be the entire vertical extent of the atmosphere north of 20°N.

c. The spectral truncation operator

A second operator, acting on the state vector spectral components, can be defined to constrain the state vector spectral characteristics, both at initial and final time.

Denote by $w(n, m)$ the following function in wavenumber space:

$$w(n, m) = 1 \quad \text{if} \quad (n, m) \in N, \tag{12a}$$

$$w(n, m) = 0 \quad \text{if} \quad (n, m) \notin N, \tag{12b}$$

where n is the total wavenumber, m is the zonal wavenumber, and N identifies a region of the spectral space. Denote by Wx the multiplication of each spectral component of the vector x by the function $w(n, m)$.

Perturbations with maximum global energy growth and with chosen wavenumber characteristics can be computed by applying the spectral truncation operator W at initial and/or final time:

$$\|x(t)\|^2 = (W_1LW_0x_0; W_1LW_0x_0) = (x_0; W_0^{*E}L^{*E}W_1^{*E}W_1LW_0x_0), \tag{13}$$

where W^{*E} is the adjoint of the spectral truncation operator W with respect to the energy inner product. Note that the operators W_0, W_1, (i.e., the spectral truncation operator applied at initial and final time) can be defined by different functions $w(n, m)$. In this paper the shape of the spectral truncation operator was taken to be a single cut in total wavenumber space, as depicted in Fig. 1 and Table 1.

The vertical distribution of the model levels used in all experiments is shown in Table 2. The averaged grid spacing in the midtroposphere is about 1 km. The effect of the vertical resolution on the experiments about horizontal scale presented in this paper is an important issue. We argue that the vertical resolution is adequate for the horizontal resolutions explored here, in part based upon experience, and in part based on the quasigeostrophic scaling argument, $L/D = N/f \approx 100$, so that our vertical resolution should be adequate for disturbances down to horizontal scales of about 500 km.

3. Scale dependence of singular vectors

a. A set of T21 calculations

We have done all nine experiments listed in Table 1 for three January dates (9 January 1993, 23 January 1993, and 2 January 1994), and each date showed the same general behavior. The total wavenumber spectra for the total energy of the singular vectors at initial time and at a final time three days later are shown in Fig. 2 for the particular case of 9 January 1993. These spectra are averages over the first 12 singular vectors calcu-

TABLE 2. Standard pressure and height values in the 19-level model.

Level number	Standard pressure (hPa)	Standard height (m)
1	10	31 055
2	29	23 972
3	50	20 571
4	73	18 169
5	102	16 038
6	140	14 018
7	190	12 105
8	251	10 321
9	325	8628
10	408	7041
11	499	5585
12	594	4279
13	689	3137
14	778	2172
15	857	1391
16	921	799
17	967	390
18	995	148
19	1009	31

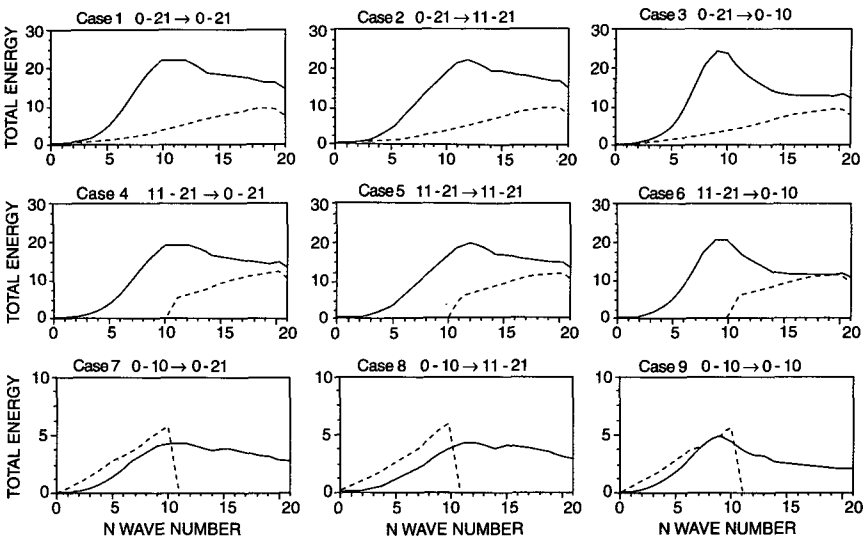

FIG. 2. Total energy as a function of spherical harmonic total wavenumber for initial (dashed) and final (solid) states of singular vectors calculated in a T21 model. The initial energy spectrum is multiplied by a factor of 100 in the top six panels and by 30 in the bottom three panels. The ordinate scale is also different for the bottom three panels. The nine panels are arranged as in Table 1. Top row: wavenumbers 0–21 present at initial time, middle row: 11–21 initial, bottom row: 0–10 initial. Left column: energy in wavenumbers 0–21 optimized at final time, middle column: 11–21 final, right column: 0–10 final.

lated at a resolution of T21 and for an optimization time of three days and optimization volume of the total mass of the atmosphere north of 20°N. The intermediate wavenumber cut is taken between total wavenumbers 10 and 11, so that $n_i = 10$. The singular vector amplitudes are normalized so that *the initial energy is always unity,* even when the energy is constrained to a limited portion of the wavenumber spectrum, so that the area under the initial energy curve is constant. Note, however, that the initial energies are multiplied by a large factor to make them easily visible in the same plot with the final energies. These spectra show several things clearly. The overall energy growth is largest when all wavenumbers are used in the initial perturbation, but limiting the initial perturbation to the upper half of the wavenumber range does not reduce the energy growth very much (compare the top row with the middle row in Fig. 2). The final state energy spectrum can be shifted toward lower wavenumbers by optimizing for the growth at low wavenumbers, but this does not increase the final state energy in the low wavenumbers by more than 10% or 20% (compare right column with left column in Fig. 2). If the initial perturbation is constrained to total wavenumbers 0 to 10, the growth of energy is greatly reduced, and more than half of the final state energy is contained in total wavenumbers greater than 10 (bottom row in Fig. 2). In cases where the high wavenumbers are present in the initial perturbation, the energy increases by a factor of about 250 in three days, whereas when only wavenumber 10 and lower are present in the initial state the total energy increases by only a factor of about 50.

It is apparent from Fig. 2 that most of the growth of energy at wavenumbers less than 11 comes from that portion of the initial perturbation that is described by wavenumbers 11 and above. It is also true that the structure of the perturbation at final time is relatively insensitive to the presence of the lower wavenumbers in the initial state, which apparently contribute little to the energy growth. Figure 3 shows the structure of the first and sixth singular vectors at initial time for the spectrally unfiltered problem corresponding to case 1 and for the case where the initial perturbation was constrained to wavenumbers greater than 10 (case 4).[2] The singular vector structures at final time for the same cases are shown in Fig. 4. For T21 truncation, the initial and final state singular vectors are both relatively insensitive to the presence or absence of total wavenumbers less than 11.

For most of the singular vectors calculated by excluding the high wavenumbers from the initial perturbation, the initial structure is more barotropic, in that less vertical tilt is evident between the lower and middle troposphere (not shown) and more of the growth

[2] We use the first and sixth singular vectors merely to illustrate that the structures are insensitive to low wavenumbers over a range of growth rates.

appears to come from meridional propagation, especially from the subtropics toward higher latitudes (Fig. 5). The structure at final time is of smaller scale because the higher wavenumbers grow from nothing to amplitudes comparable to those of the low wavenumbers. For the case shown, the energy growth has been optimized for total wavenumbers less than 11 at both initial and final time, but the final structure is not greatly different if the final energy is optimized without a wavenumber constraint (not shown), although the ordering of the singular vectors may change.

b. *T42 calculations*

Since the T21 calculations described thus far indicate a very important role for small spatial scales in forming disturbances that will grow rapidly, it is of great interest to investigate calculations at higher horizontal spatial resolution. Wavenumber energy spectra show that growth in a T42 calculation is about twice that in the T21 calculation for the particular dissipation values we have used (Fig. 6), which further corroborates the importance of small scales for producing energy growth. This doubling of the amplification factor holds approximately for each of the first 10 singular vectors and varies little from case to case (not shown). The initial energy spectrum in the unconstrained T42 case ceases, however, to increase with increasing wavenumber above about total wavenumber 21, so that one gets the impression that T42 does a better job of resolving the relevant scales, especially for energy in the synoptic scales ($n < 21$ or so). This is consistent with the further observation that when only the top half of the wavenumber spectrum ($n > 21$) is included in the initial perturbation for the T42 case, the fractional reduction in the growth of the synoptic-scale waves ($10 < n < 21$) is much more than in the case where the upper half of the spectrum ($n > 10$) is excluded in a T21 calculation.[3] We are tempted to speculate that the importance of the highest resolved wavenumbers for linear growth may decline as their scale becomes significantly smaller than the Rossby radius of deformation, which is the scale at which baroclinic energy exchanges are most efficient. To investigate this speculation would require experiments with higher resolution, which we have been unable to do because of the substantial computational requirements. Moreover, the horizontal Rossby radius of deformation in a stratified flow ($L_R = ND/f$) depends also on the vertical scale of the disturbance, which cannot be specified a priori. Therefore, the growth rate of disturbances with a particular horizontal scale depends also on the vertical resolution available. An example of the relationship between ver-

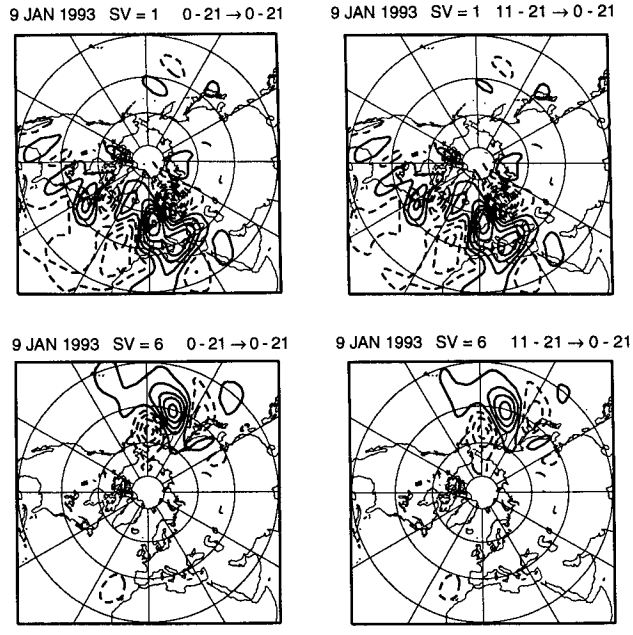

FIG. 4. The same as Fig. 3 except for the singular vectors at final time (3 days) and at model level 11 ($p \approx 499$ hPa). The amplitude scaling is relative to that in Fig. 3, and the same for all cases. The contour interval is 20 times that in Fig. 3.

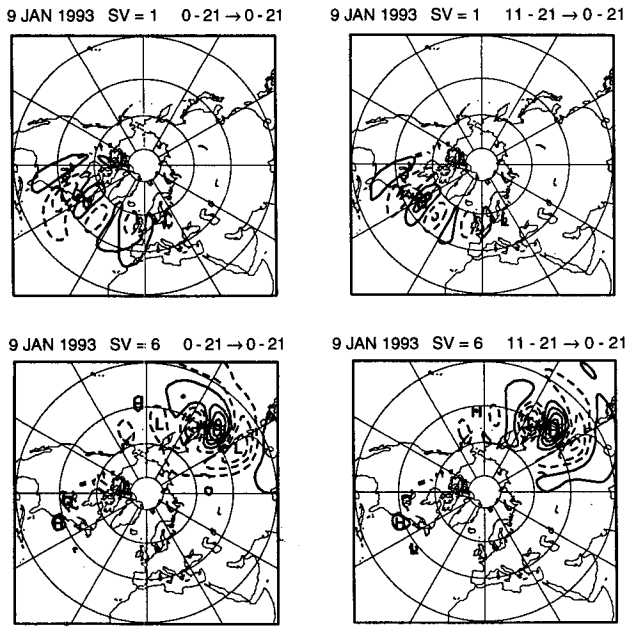

FIG. 3. Streamfunction at model level 15 ($p \approx 857$ hPa) of the first (top) and sixth (bottom) singular vectors at initial time for the spectrally unconstrained case in which initial and final energies are optimized for total wavenumbers 0–21 (left) and for the case in which the input singular vector energy is confined to total wavenumbers 11–21 (right). The initial date is 9 January 1993. The amplitude scaling is arbitrary, but the same for all four panels. Dashed contours indicate negative values.

[3] One must consider the fact that the highest wavenumbers are more strongly damped in the T42 calculations, however.

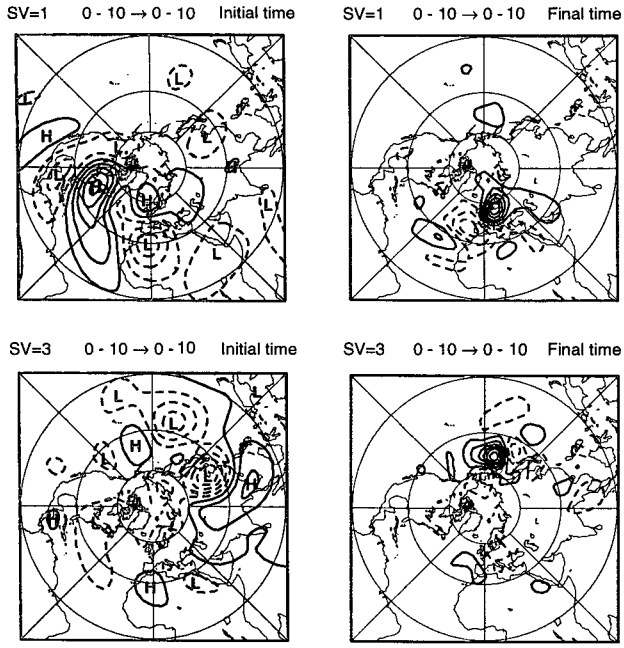

FIG. 5. Streamfunction at model level 11 ($p \approx 499$ hPa) of the first (top) and third (bottom) singular vectors at initial time (left), for the case in which initial and final energies are optimized for total wavenumbers 0–10 (bottom-right column of Table 1) and the final states of these singular vectors (right) for the initial date 9 January 1993. Note that the outermost latitude circle is the equator in this figure, whereas it is 20°N in Figs. 3 and 4. The contour interval on the right is 10 times that on the left.

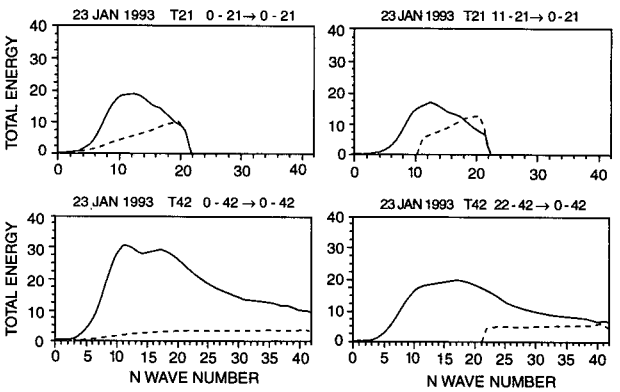

FIG. 6. Total wavenumber energy spectra at initial and final time as in Fig. 2 except for the case of 23 January 93 and averaged over the first 10 singular vectors. The upper two panels show spectra calculated at T21 resolution and the lower two panels show T42 spectra. The panels on the left show the spectra for the case in which no spectral constraint is applied to the optimization problem, and the panels on the right show cases in which the initial energy is confined to the upper half of the spectrum, 11–21 for the T21 calculation (top) and 22–42 for the T42 calculation (bottom). The initial energies are multiplied by 100 so that they can be seen.

tical and horizontal scale for growing disturbances in the context of these calculations is shown below. The sensitivity of linear growth to further increases in both vertical and horizontal resolution is a very interesting and important issue that we cannot adequately address here.

The vertical distributions of energy in the initial and final states for the unconstrained T21 and T42 calculations are shown in Fig. 7. The energy of the initial perturbation is confined near the effective steering level and then propagates[4] both upward and downward away from the steering level to achieve energy growth, which is consistent with expectations derived from the theory of wave action, since as the wave propagates into a region of larger Doppler-shifted frequency, the energy of the wave should increase (e.g., Bretherton and Garrett 1968; Tung 1983; Buizza and Palmer 1995). For a particular resolution, the vertical distributions of initial and final energy are not very sensitive to total wavenumber filtering, but the distribution of energy at final time does vary somewhat from day to day. For example, the T21 calculation for 3 January 1994 has a vertical energy distribution at final time more like that of the T42 calculation on 23 January 1993, so one can speculate that the state of the atmosphere on 3 January 1994 is more favorable to the growth of low-level disturbances than it is on 23 January 1993. The T42 cal-

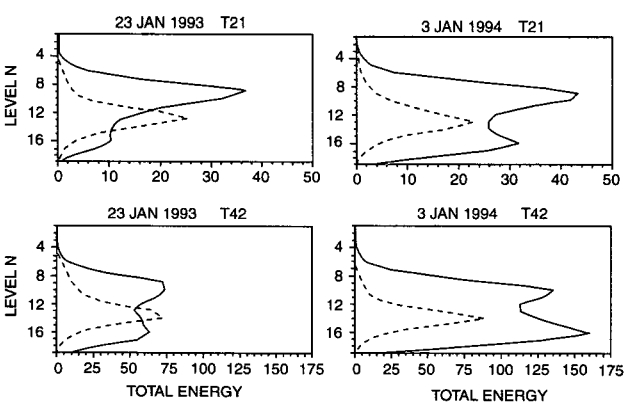

FIG. 7. The initial (dashed) and final (solid) total energy in the spectrally unconstrained T21 (top) and T42 (bottom) calculations, averaged over the first 10 singular vectors, and plotted as functions of model level number for the case of 23 January 1993 (left) and 3 January 1994 (right). The sigma surfaces corresponding to these model levels are given in Table 2. Initial energies are multiplied by 100 for T21 and 300 for T42.

[4] Although the singular-vector wave packet consists of a range of wavenumbers and phase speeds, it does appear to have a characteristic phase speed over its three-day life, so that the concept of steering level has some value. We use *propagate* in the loose sense that the location of most energy content of the singular vector moves from one region to another as it develops. Most of the energy change is growth rather than conservative transport, of course, although propagation of pseudomomentum or wave action might be a good description of what happens.

culation for 3 January 1994 shows even greater low-level development than the T21 calculation for the same date, so that the greater prominence of low-level development in higher-resolution calculations appears in both cases presented, and also in the 9 January 1993 case (not shown).

The downward propagation is more prominent in the T42 calculation, perhaps because the shallow disturbances associated with this low-level energy growth are of smaller horizontal scale. We expect the horizontal (L) and vertical (D) scales of quasigeostrophic disturbances to maintain a ratio that is similar to that of the Brunt–Väisälä frequency (N) to the Coriolis parameter (f):

$$\frac{L}{D} = \frac{N}{f}, \tag{14}$$

so that as the horizontal scale becomes smaller, so must the vertical scale. Support for this hypothesis is gained by comparing the vertical and spectral energy structure for individual singular vectors. If we compare modes that grow predominantly in the upper troposphere with those that grow more in the lower troposphere, we find that the latter have more high wavenumber energy in the final state. An example is shown in Fig. 8 for the case of 23 January 1993. The second singular vector has strong energy growth below the steering level, which peaks between total wavenumbers 15 and 20. The fifth singular vector has greater energy growth above the steering level and has a final energy spectrum that is peaked near total wavenumber 11.

The singular vectors calculated at T42 are of smaller horizontal scale than those calculated at T21, as expected, but if the lower half of the total wavenumber spectrum is eliminated in the calculation of the singular vectors, there is a greater change in structure than when wavenumbers 0–10 are eliminated from the singular vector at initial time in the T21 case (Fig. 9). The structure is very similar, but there is a significant contribution from wavenumbers 0–21. At final time, the differences are smaller, however, indicating that much of the structural information in the T42 singular vectors originates at wavenumbers greater than 21 (Fig. 10). The insensitivity of the singular vector structure to the presence or absence of the synoptic scales in the initial structure may be provided by the linear propagator (3) itself, which contains information about the basic flow trajectory at all scales.

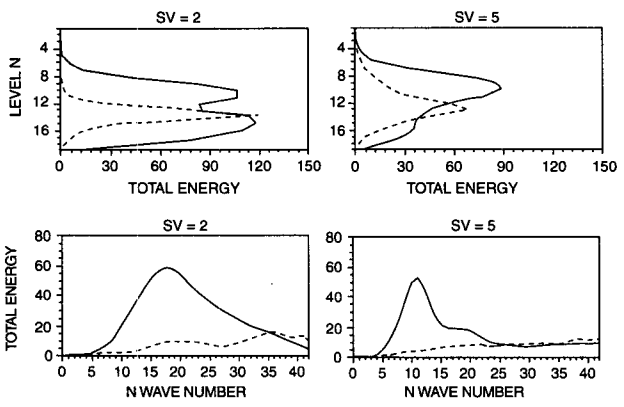

FIG. 8. The vertical and spectral distribution of energy in the initial (dashed) and final (solid) states of the second (left) and fifth (right) singular vectors calculated at T42 resolution for 23 January 1993. Initial energies are multiplied by 300 to make them visible.

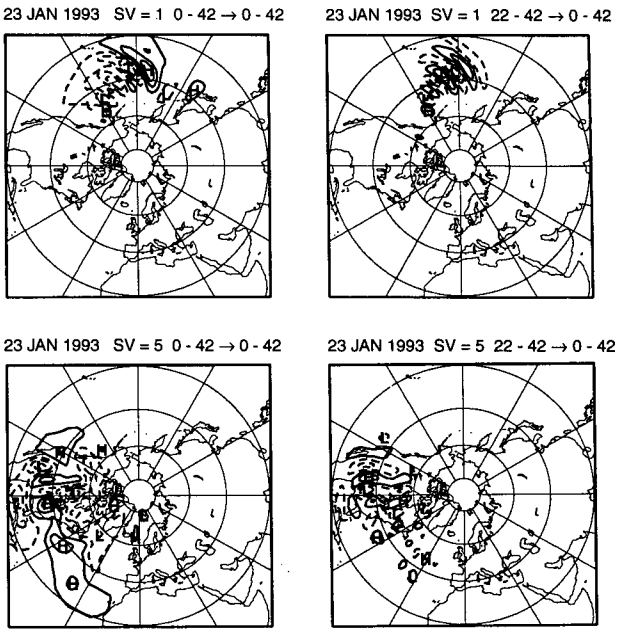

FIG. 9. The singular vector streamfunction at initial time at model level 15 ($p \approx 857$ hPa) for singular vectors 1 (top) and 5 (bottom) calculated with the initial energy at all wavenumbers (0–42, left) and calculated with the initial energy confined to the top half of the spectrum (22–42, right). The initial date is 23 January 1993. Dashed contours are negative.

4. T63 nonlinear integrations

We investigate here the possibility that low-wavenumber disturbances, while exhibiting rather modest linear growth, may be of greater importance in the nonlinear regime of flow because of a strong interdependence with the baroclinic eddies, that both respond to the large wavenumber flow and modify it through generating potential vorticity fluxes and latent heating. To look at this idea we have performed a number of integrations using a T63 version of the ECMWF prediction model with full physics (Cycle 46). A series of integrations were initiated from the same date by perturbing the initial condition by adding individual singular vectors with their amplitude set to unit total energy. This amplitude corresponds approximately to current estimates of the analysis error in initial conditions used in ECMWF forecasts. We used the first six

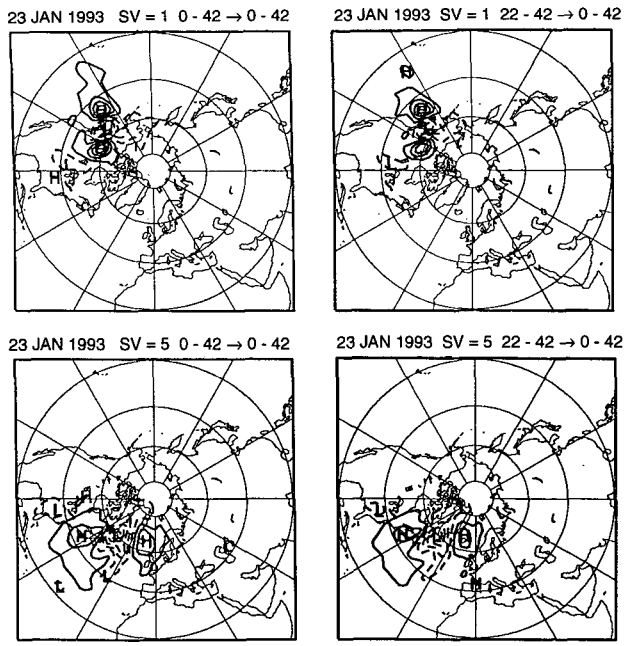

FIG. 10. Same as Fig. 9 except for the singular vector at final time (day 3) and at level 11 ($p \approx 499$ hPa). The contour interval is 50 times that in Fig. 9.

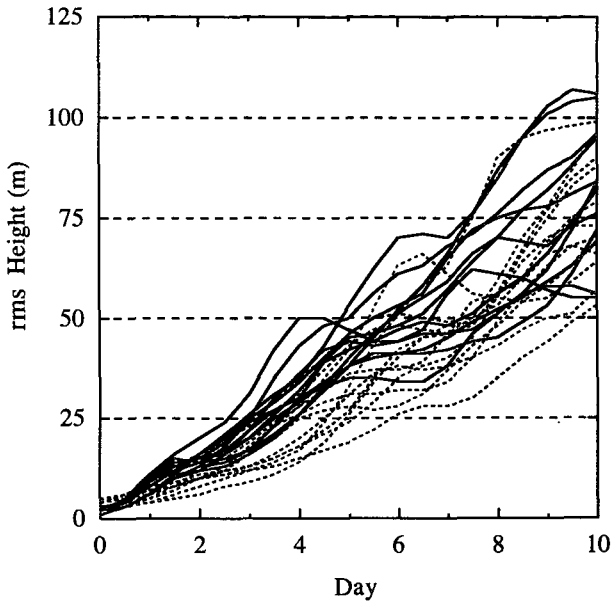

FIG. 11. The rms 500-hPa height deviation from the 9 January 1993 control forecast over the Northern Hemisphere of 12 ensemble forecasts for the spectrally unconstrained singular vector perturbations (solid lines) and for the case in which the initial and final energies were optimized for wavenumbers less than 11 (dashed lines) plotted as functions of forecast day.

singular vectors, each with positive and negative sign for a total of 12 perturbed experiments plus an unperturbed control experiment. We then calculated the rms (root mean square) deviation between perturbed forecasts and the control integration, using the 500-hPa height field over the Northern Hemisphere as the comparison standard. The result is as expected from the linear calculation. The low-wavenumber perturbations grow more slowly, show less dispersion, and less variation from the control integration through most of the 10-day forecast period, but especially during the first 5 or 6 days (Figs. 11 and 12). Figure 11 shows the growth of rms amplitude over the Northern Hemisphere, and Fig. 12 shows the maximum local height deviation at any point. Experiments in trying to improve forecasts using singular vector perturbations of the initial condition also show that the high wavenumber perturbations are much more effective because they foster more rapid growth at the relevant scales. Low wavenumber perturbations induce rapid energy growth by fostering perturbations at smaller scales (Figs. 2 and 5) and so are not self-perpetuating but give rise to synoptic-scale wavetrains downstream. These downstream synoptic wavetrains are smaller in amplitude when the initial perturbations are confined to low total wavenumbers, or equivalently to large spatial scales.

In summary, optimally configured disturbances of small spatial scale and small initial amplitude give rise to synoptic-scale disturbances that can substantially alter the nonlinear evolution of the flow field. Optimally configured perturbations that are confined to larger spatial scales are much less effective in altering the flow evolution. The low wavenumber perturbations also

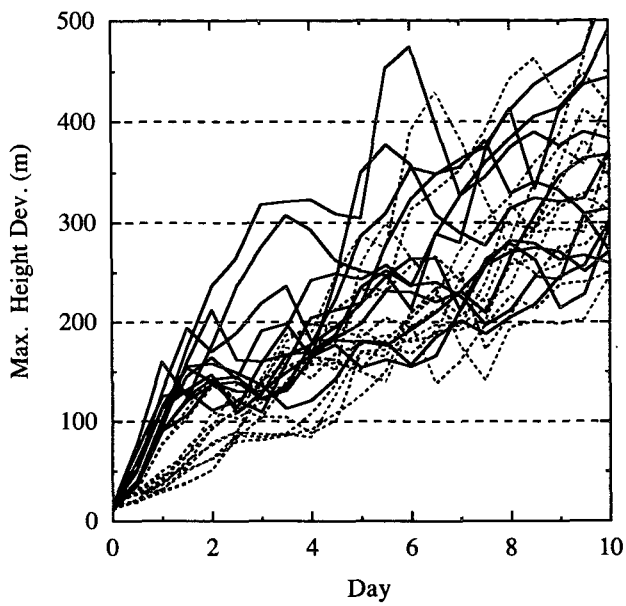

FIG. 12. Same as Fig. 11 except for the maximum difference at any point of the 500-hPa height field between an ensemble member and the control forecast.

give rise to synoptic-scale disturbances, but their growth is much slower than when small-scale initial perturbations are used, and they remain less important long after the period of linear growth is past.

5. Conclusions

The singular vectors of a numerical weather prediction model are defined as those perturbations that, when acted on by the linear tangent operator of the model, will experience the most rapid linear growth over some finite period. Using a total wavenumber filter in the energy growth optimization problem, we have been able to study how linear growth depends on the scale of the initial and final structures. Linear growth of small disturbances to realistic tropospheric flows is most rapid for the smallest scales contained in models truncated at T42 or less. Disturbances composed of subsynoptic-scale wavenumbers may very rapidly grow to synoptic-scale waves of large amplitude. The information for the final synoptic-scale structure is contained in the subsynoptic wavenumbers, since the structure of the singular vector at final time is insensitive to the presence or absence of the large scales in the initial perturbation. The vertical structure also evolves from very baroclinic structures confined near the steering level to more barotropic structures occupying the whole troposphere. In some cases growth below the steering level is favored, and these disturbances tend to have smaller spatial scales at final time than disturbances that grow predominantly in the upper troposphere. The relationship between vertical and horizontal scale is hypothesized to be related to the need for disturbances to maintain quasigeostrophic balance between Coriolis forces and pressure forces associated with adiabatic vertical displacements ($fL \sim ND$).

Singular vectors constrained to be of large scale at initial time grow much more slowly than unconstrained, smaller-scale perturbations. These large-scale initial perturbations tend to be more barotropic in structure, and growth by barotropic mechanisms is more important. Integrations of the ECMWF forecast model with initial perturbations consisting of singular vectors show much less forecast dispersion when low-wavenumber singular vectors are added than when high-wavenumber singular vectors with the same initial energy are used to perturb forecasts.

The results shown here suggest that, for a three-day optimization time, the fastest energy growth is achieved with initial perturbations that are subsynoptic in scale and that these perturbations quickly assume the structure of synoptic-scale waves. If T42 resolution is used in the singular vector calculation instead of T21, then the growth rates are higher (about double for the dissipation we used) and the spatial scale at both initial and final time is smaller. It is of great fundamental interest for numerical weather prediction to determine whether linear growth rates continue to increase with resolution, and, if so, at what rate. In this regard, the sensitivity to vertical resolution and the effect of physical processes such as diffusion and physical processes need also to be investigated. If the growth rates continue to increase at smaller and smaller spatial scales, then this may imply very stringent requirements on the knowledge of fine spatial detail in initial fields in order to make accurate deterministic weather forecasts beyond a few days time. If the growth rates or the rate at which energy is transferred from subsynoptic to synoptic scales begin to decline significantly as the spatial scales become smaller and smaller, then the requirements may be less severe.

Acknowledgments. The authors benefited by discussing this work with A. Hollingsworth, B. J. Hoskins, F. Molteni, A. Simmons, and S. Webster. Candace Gudmundson edited the manuscript, and Kay Dewar helped draft the figures. This work was conducted at the European Centre for Medium-Range Forecasts while DLH was a visitor there. Additional support for DLH was provided by the Climate Dynamics Program of the National Science Foundation under Grant ATM-9313383.

REFERENCES

Borges, M. D., and D. L. Hartmann, 1992: Barotropic instability and optimal perturbations of observed nonzonal flows. *J. Atmos. Sci.*, **49,** 335–354.

Boyd, J. P., 1983: The continuous spectrum of linear Couette flow with the beta effect. *J. Atmos. Sci.*, **40,** 2304–2308.

Bretherton, F. P., and C. J. R. Garrett, 1968: Wavetrains in inhomogeneous moving media. *Proc. Roy. Soc. London,* **A302,** 529–554.

Buizza, R., 1994: Sensitivity of optimal unstable structures. *Quart. J. Roy. Meteor. Soc.*, **120,** 429–451.

——, and T. N. Palmer, 1995: The singular-vector structure of the atmospheric general circulation. *J. Atmos. Sci.*, **52,** 1434–1450.

——, J. Tribbia, F. Molteni, and T. N. Palmer, 1993: Computation of optimal unstable structures for a numerical weather prediction model. *Tellus,* **45A,** 388–407.

Courtier, P., C. Freydier, J.-F. Geleyn, F. Rabier, and M. Rochas, 1991: The Arpege project at Météo-France. *Proc., Numerical Methods in Atmospheric Models,* Shinfield Park, Reading, United Kingdom, ECMWF, 193–231.

Farrell, B. F., 1982: The initial growth of disturbances in a baroclinic flow. *J. Atmos. Sci.*, **39,** 1663–1686.

——, 1989: Optimal excitation of baroclinic waves. *J. Atmos. Sci.*, **46,** 1193–1206.

Lacarra, J.-F., and O. Talagrand, 1988: Short-range evolution of small perturbations in a barotropic model. *Tellus,* **17,** 321–333.

Lorenz, E. N., 1963: The predictability of hydrodynamic flow. *Trans. New York Acad. Sci., Ser. 2,* **25,** 409–432.

Molteni, F., and T. N. Palmer, 1993: Predictability and finite-time instability of the northern winter circulation. *Quart. J. Roy. Meteor. Soc.*, **119,** 269–298.

Noble, B., and J. W. Daniel, 1977: *Applied Linear Algebra.* Prentice-Hall Inc., 477 pp.

Tung, K. K., 1983: Initial value problem for Rossby waves in a shear flow with critical level. *J. Fluid. Mech.*, **133,** 443–469.